

Electronic transport modulation on few-layers suspended MoS₂ under strain

Igor Neri and Miquel López-Suárez

*NiPS Laboratory, Dipartimento di Fisica e Geologia,
Università degli Studi di Perugia, 06123 Perugia, Italy**

(Dated: January 21, 2020)

Abstract

The production of new sensors, transducers and electronic components can benefit from the possibility to alter the electronic transport of metal-semiconductor-metal (MSM) devices. 2D materials are extremely appealing for those new technologies. This can be determined by several phenomena as piezoelectric effect, piezoresistive effect and modulation of Schottky barrier. In particular, MoS₂, among other Transition Metal Dichalcogenides (TMDs), is predicted to show a transition from semiconductor to metal under strain. In this article we present measurements on the modulation of electronic transport on few layer MoS₂ suspended ribbons under uniaxial tensile strain. Experimentally observed changes in the two terminal IV curves can be explained in terms of band gap closing in the semiconductor. A maximum gauge factor of 240 is achieved for a 3-layer ribbon. We also report on the fabrication process that allows to apply high strains to suspended MoS₂ ribbons, paving the way to future studies on the effect of strain in 2D materials.

* igor.neri@nipslab.org, miquel.lopez@nipslab.org

I. INTRODUCTION

The study of the electronic properties of nanostructured materials has gained a lot of interest in the last years. Nanowires, thin films and nanoribbons have been considered as the base for applications as sensors [1], transducers [2], energy harvesters [3] and electronic components [4]. 2D materials are foreseen to be particularly interesting for such applications because of their outstanding optical, mechanical and electrical properties along with very strong electro-mechanical and opto-mechanical coupling[5–7]. Graphene, hexagonal Boron Nitride (h-BN) and Transition Metal Dichalcogenides (TMDs) are examples of such materials.

Molybdenum disulphide, MoS_2 , is a layered crystalline TMD with an hexagonal structure. Single layer MoS_2 is formed by a plane of Mo atoms sandwiched and covalently bonded to two planes of S atoms. Few layer and bulk MoS_2 is formed by successive stacking of this hexagonal structure through vdW forces. In contrast with graphene, MoS_2 , along with the rest of TMDs and h-BN, is non centrosymmetric and has been theoryzed to show macroscopic polarization under mechanical strain [8]. This property would be present (absent) for odd (even) layered ribbons. Recently, the piezoelectric response of MoS_2 has been experimentaly measured [7, 9] along with the first experimental insights on its piezoresistive response, indicating a sort of band gap modulation under mechanical deformation. MoS_2 has been suggested to show a transition from semiconductor to metal under mechanical strain[10–13] and not only for monolayer MoS_2 but also for few-layer MoS_2 , and even for its bulk form[14, 15], which is partially supported by experimental data from Ref. 7. In its bulk form, MoS_2 is a semiconductor with indirect band gap and $E_g=1\text{ eV}$, while its single layer counterpart shows a direct transition at the K point with $E_g=1.9\text{ eV}$. The band structure of MoS_2 is also influenced by the Schottky barrier that arise when in contact with a metal. The contribution of the Schottky barrier to the energy band-gap is expected to be of $0.06 - 0.16\text{ eV}$ for Au- MoS_2 contacts[16].

In this work we report measurements of the change in electronic transport on few-layers suspended MoS_2 under tensile strain. Such behaviour can be accounted to the reduction of the energy band gap of the semiconductor and modulation of the Schottky barrier. Changes in the direct-current electronic transport are characterized for a set of MoS_2 suspended ribbons under uniaxial tensile strain. A drastic increment in the current flowing through the

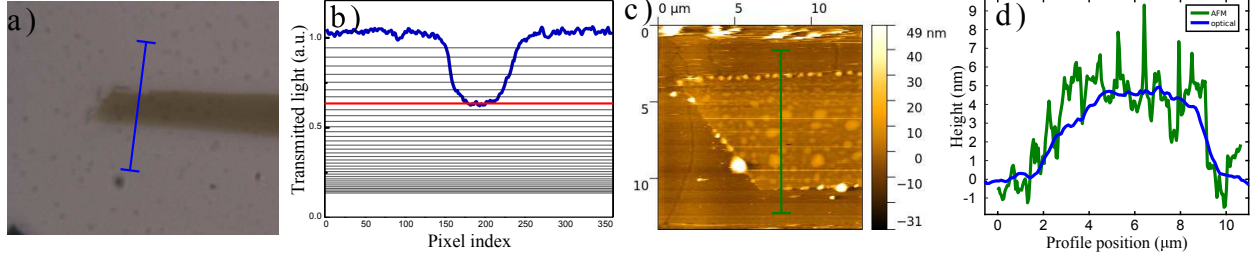


FIG. 1. Optical and AFM characterisation of a MoS₂ flake. a) Image under an optical microscope in light transmittance of a flake on PDMS. b) Estimation of the number of layers, n , based on the light transmittance of single layer MoS₂, corresponding to $n = 8$. c) AFM measurement of the flake on the Au/Cr coated (55 nm) 500 μm SiO₂ substrate. d) Height profile of the flake reconstructed from AFM image and light transmittance analysis.

device is obtained when the material is effectively strained. The results and the methodology shown in this work pave the way for the development of micro and nanodevices exploiting the strong electro-mechanical coupling of MoS₂ such as strain sensors or straintronic devices, among others. In particular such strain induced semiconductor-conductor transition can be exploited to realize transistors where the gate is represented by the applied strain. In this prospective it is possible to imagine hybrid flexible computing devices that get the input from the human body movements (strain) producing an electrical output.

II. METHODS

MoS₂ flakes are obtained by mechanical exfoliation from a single crystal [17, 18] with the “scotch tape method” and then transferred to a polydimethylsiloxane (PDMS) holder as in Ref. 19. An optical microscope is used to locate few layer MoS₂ candidates for the analysis. To estimate the number of layers we have performed an optical analysis considering the light transmittance of single-layer MoS₂ to be 94.5% [20]. The overall transmittance of the flake decreases with the number of layers following a power-law[20]. An optical image of one of the flakes (s_2) is reported in Fig. 1 along with its transmittance profile and AFM measurement. Each horizontal gray line in the light transmittance profile is relative to the expected value for a specific number of layers, starting from the top line corresponding to a single layer, $n=1$. The red curve corresponds to the transmitted light for the estimated number of layers for the MoS₂ flake ($n = 8$). The validity of the optical analysis is corroborated by AFM

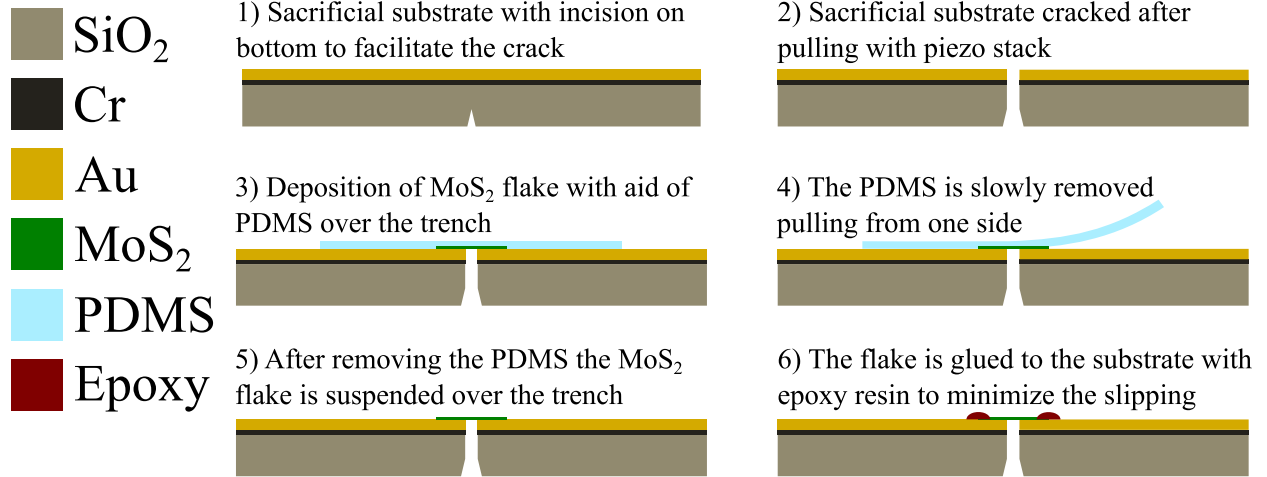


FIG. 2. Schematic representing the preparation of the hospital substrate and deposition of the MoS_2 flake.

measurements reported on the third panel along with the estimated height from the optical analysis. The good agreement between the AFM measurement and the estimated height highlights the reliability of the layers estimation method from light transmittance. Optical images and analysis of the other flakes are reported in Supplementary Material.

The hospital substrate for the sample consists on a Au/Cr coated (55 nm) 500 μm SiO_2 wafer. Before transferring the flakes each substrate has been mounted on a high precision nanopositioning stage clamping one end to the reference frame and the other to the movable part. The positioning system is capable of a maximum extension of 35 μm with a pull force of 10 N. An incision is made on the bottom of the substrate (see panel 1 in Fig. 2) in order to split it in two parts with a clean crack by means of the force applied by the piezoelectric stage. The two independent parts are then separated by a initial gap g defining the two electrical contacts of the device. Selected flakes are transferred over the trench once the initial gap is set to $g = g_0$ where g_0 is the gap at which the current through the contacts, before transferring the flake, is less than 0.01 nA, negligible for the expected current passing through the device. This sets the length of the metal-semiconductor-metal (MSM) device to $l = g_0$.

The overall procedure for the preparation of the hospital substrate and deposition of the flake is presented in Fig. 2 (see Supplementary Material for pictures taken during the flake transferring). It has to be noted that the application of strain to the suspended

TABLE I. Parameters of the measured samples.

Sample	$l(\mu m)$	$w(\mu m)$	n	$A_L(\mu m^2)$	$A_R(\mu m^2)$	Clamped
s_1	4.96	6.7	3	23.9	165.6	no
s_2	7.14	11.7	8	385.8	674.8	no
s_3	3.07	9.43	7	321.2	245.6	no
s_4	6.16	7.28	6	-	-	yes
s_5	9.2	2.92	7-bulk	-	-	yes

ribbon is a difficult task that can be influenced by different factors. In particular, the capacity to apply an effective strain depends on the adhesion forces between the flake and the substrate. If strain overcomes the adhesion forces the sample may slip over the contacts reducing drastically its internal strain. To tackle this problem it is possible to anchor the ends of the flake to the substrate (see panel 6 in Fig 2). However, this procedure may introduce additional strain even orthogonal to the gap opening direction that cannot be easily removed. For this reason we have conducted the experiments in both configurations, with and without anchoring. Table I shows the main parameters of the devices.

To observe the modulation of the electronic transport as effect of applied strain we measured the current flowing through the material varying the polarization V_p in a two terminal configuration, *i.e.* the IV curve. We recall here that applying tensile strain to MoS₂ results in a reduction of its energy band-gap up to the point of reaching a transition from semiconductor to metal (semi-metal for multilayer MoS₂). An additional collateral effect of the strain can be the modulation of the Schottky barrier height[21].

Strain is applied to the MSM device by increasing the gap, g . The effective length of the gap is directly measured through the integrated positioning sensor of the linear actuator which has a resolution of 0.2 nm.

While in a digital simulation strain is uniformly applied along one or more dimensions of the device, in a real scenario small imperfections on the material itself, or the exact orientation in which the flake has been transferred to the host substrate can produce a non uniform distribution of strain. In order to know exactly the strain applied to the device a local measure with Raman and/or Photoluminescence spectroscopy should be considered, which is unfeasible for the current setup. In our experiments the strain is thus roughly

estimated as $\epsilon = g/g_0 - 1$, where g is the measured value of the gap, which bounds the effective maximum strain. For non clamped devices the estimated strain can be larger than the real one due to possible slippage of the sample over the substrate.

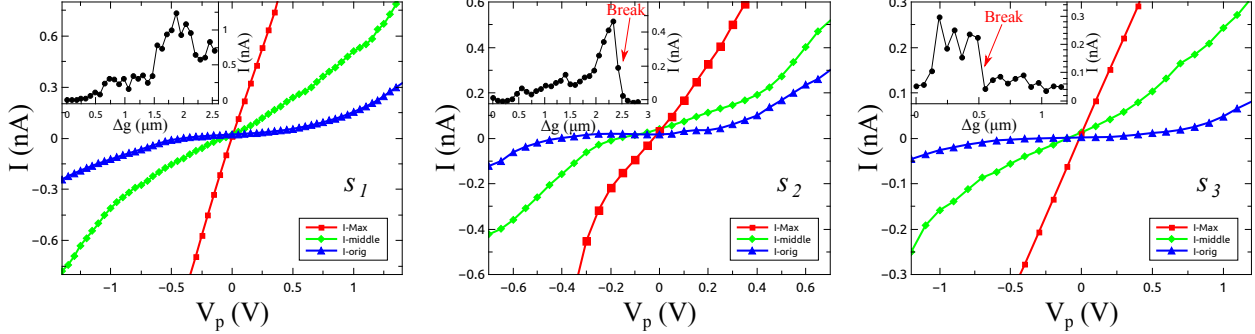


FIG. 3. Current-voltage relation as a function of applied tensile strain for s_1 , s_2 and s_3 . IV curves for the three unstrained devices are represented by blue triangles. The steepest IV curves, achieved at strains ranging from 15% to 20%, are represented by red squares. A linear relation is achieved for s_1 and s_3 . Data corresponding to intermediate strains are showed with green circles. Insets show the current at fixed polarization voltage, $V_p = 300$ mV, as gap increases. The rupture of the structure, highlighted with red arrows, corresponds to a drastic diminution of the current.

III. RESULTS AND DISCUSSION

We start our analysis with the not clamped devices. In Fig. 3 we show the two terminal IV curves for the three samples, s_1 , s_2 and s_3 , for three different strain levels: no strain, moderate strain, maximum strain. The typical semiconductor behaviour is observed for the pristine configuration (blue triangles): a linear relation in the IV curve at low bias voltage followed by a change in the slope at large biases.

Each inset in Fig. 3 shows the current flowing through the corresponding device at $V_p = 300$ mV as g is increased. For the first sample it can be seen that, starting from $g = g_0$, the current increases as the gap is opened. In these first stretching steps the current reaches a value 2 orders of magnitude higher than this for $g = g_0$. Samples s_2 and s_3 show similar qualitative trends but with a lower increase in the current of a factor 10 and 20, respectively. The IV curves show that the increment of flowing current is accompanied by a linearisation of the IV relation, which can be explained in terms of energy gap closing although Schottky

barrier height modulation cannot be excluded. Specifically, sample s_1 and sample s_3 show an increment in the slope of the IV curve from 0.042 nA/V to 2.15 nA/V and from 0.0083 nA/V to 0.72 nA/V, respectively. Sample s_2 equally shows an increment of more than two orders of magnitude, from 0.0085 nA/V to 1.30 nA/V yet preserving a non linear relation. During strain application, MoS₂ flakes may slip over the Au contacts releasing part of the mechanical energy stored in the system recovering an electric response corresponding to a less strained state. Such events are visible on all insets of Fig. 3 as a drop on the current. The maximum strain that a device can support before slippage or rupture depends on several factors. Among them, the contact area between the flake and the substrate is expected to play an important role [22]. The areas of the left(right) contacts, $A_L(A_R)$, are reported on Table I for the non clamped samples. For sample s_1 , A_L is much smaller than A_R , and much smaller than the ones of the other samples. The reduced contact area favors potential slippage of the sample. As evident in the inset of panel (a) of Fig. 3, during the last steps of the experiment, the current flowing through the device decreases, which may be caused by the slippage of the left contact. The presence of slippage is confirmed by analyzing the optical images of the devices taken during the experiment. The detected slippage can be correlated with the drop in the current corroborating the dependence of the increase in current flowing through the device with applied strain (see Supplementary Material for slippage analysis). This is accompanied also with a further reduction of the current due to a smaller contact area. Instead, sample s_2 and sample s_3 have much larger contact areas that helped preventing slippage, in this scenario during the application of the strain the flakes broke in the final steps as indicated with red arrows in Fig. 3.

In order to prevent slippage, we have repeated the measurements with two samples this time clamping both ends of the suspended flakes with epoxy resin, as depicted on panel 6 of Fig. 2. The same procedure for strain application is followed for these samples. The results are presented in Fig. 4. For both samples the pristine semiconductor IV curve became steeper as strain is applied. However, sample s_4 still preserves a non linear IV relation even for the most strained states even if the IV curve is steeper in the central region reaching a maximum increment in the current at $V_p = 300$ mV of a factor 2. Sample s_5 , composed by a bulk/7-layer heterostructure, presents more interesting features. In particular, the IV curve reached a linear relation for the maximum strain. Moreover, at fixed $V_p = 300$ mV, the current is a monotonic function of the gap, suggesting that anchoring effectively prevents

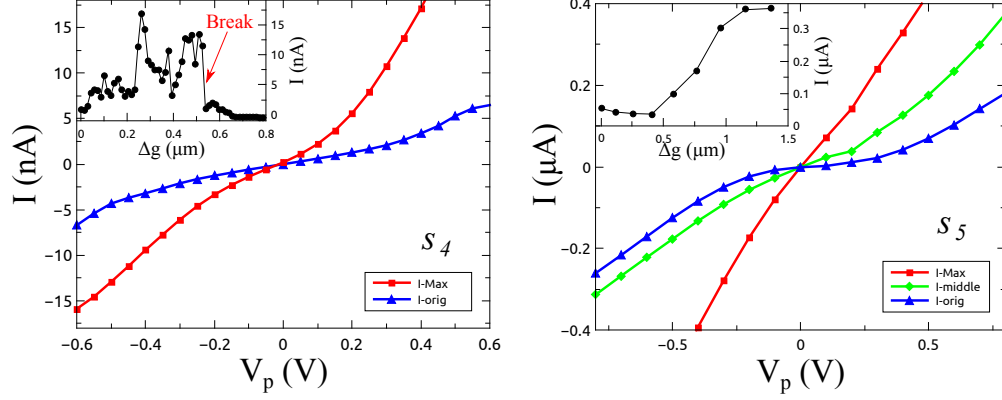


FIG. 4. Current-voltage relation as a function of applied tensile strain for s_4 and s_5 . IV curves for the two unstrained devices are represented by blue triangles. The steepest IV curves are represented by red squares. A linear relation is achieved for s_5 while s_4 preserves a non linear response even if it shows a moderate current increase. Data corresponding to an intermediate strain are shown with green circles for s_5 . Insets show the current at fixed polarization voltage, $V_p = 300$ mV, as gap increases. A rise of the current is observed for both devices although for s_4 the increment is lesser than an order of magnitude. The rupture of s_4 is highlighted with a red arrow.

slippage over the contacts. The presence of the bulk material contributes to the mechanical stability of the few layer part of the ribbon, which reflects on less noisy data, while its contribute to the electronic transport can be neglected (see Supplementary Material for IV curve of the bulk part).

For samples s_1 and s_5 it is possible to estimate the applied strain as function of gap aperture and thus these samples give the opportunity to design and analyze the equivalent circuit of the measured device. A model of the equivalent circuit is presented in Fig. 5(a). R_C represents the contact resistances, Z_b the background impedance that accounts for the bulk MoS₂, for sample s_5 , and parasitic currents. Finally, $Z_{\text{MoS}_2}(\varepsilon)$ is the strain dependent impedance of the MoS₂ flake. According to the presented model the total conductance of the device can be expressed as:

$$G(\varepsilon) = \frac{G_R (G_{\text{MoS}_2}(\varepsilon) + G_b)}{G_R + G_{\text{MoS}_2}(\varepsilon) + G_b} \quad (1)$$

where the conductance G_x is the inverse of the impedance Z_x . Within this model the modulation of the Schottky barriers is neglected and only the MoS₂ conductance has a direct dependence with strain. According to Ref. 23 the conductance of a semiconductor

TABLE II. Fitted parameters from the conductance model for sample s_1 and s_5 .

Parameter	s_1	s_5
R_C	$310.7 \times 10^6 \Omega$	$1.02 \times 10^6 \Omega$
Z_b	$1.67 \times 10^{10} \Omega$	$8.24 \times 10^6 \Omega$
G_0	$2.94 \times 10^{-12} \text{ S}$	$13.05 \times 10^{-10} \text{ S}$
$\partial E_g / \partial \varepsilon$	$-31 \text{ meV}/\% \text{ strain}$	$-45 \text{ meV}/\% \text{ strain}$

under strain can be expressed as

$$G_{\text{MoS}_2}(\varepsilon) = G_0 \exp \left[-\frac{\varepsilon}{2k_B T} \frac{\partial E_g}{\partial \varepsilon} \right] \quad (2)$$

where G_0 stands for the conductance of the unstrained MoS₂ flake, k_B is the Boltzmann constant and T is the temperature. The measured conductances of the devices are represented by black dots in Fig. 5(b) and (c) for sample s_1 and s_5 , respectively. The model defined by Eq. 1 and Eq. 2 is used to fit experimental data showing a good agreement. The fitting parameters for the two samples are reported in Table II, which agree with the literature[23]. In particular the model gives an energy gap modulation of $-31 \text{ meV}/\% \text{ strain}$ for s_1 and $-45 \text{ meV}/\% \text{ strain}$ for s_5 , close to the rate obtained from *ab initio* calculations ($-50 \text{ meV}/\% \text{ strain}$)[14, 15].

We have calculated the gauge factor for the four MSM devices that achieved a linear IV relation (s_1, s_2, s_3 and s_5) at $V_p=300 \text{ mV}$ ($[\Delta I(\varepsilon)/I(0)]/\Delta \varepsilon$). For s_1 we have obtained 240 in the range 0-20% of strain. For s_2 and s_3 the corresponding gauge factors are 58 and 71 in the 0-15% range, respectively. Finally for s_5 the gauge factor is 118 in the range 5-10% of strain. The obtained values for all samples exceed the values of conventional and other 2D based strain sensors, like graphene based devices[24].

IV. CONCLUSIONS

In conclusion, we have measured the changes in the electronic transport of few-layer MoS₂ ribbons under monoaxial tensile strain. An increase of more than an order of magnitude of the current flowing through the device and a linear IV relation are obtained for several devices at strains ranging from 10% to 20%. A maximum gauge factor of 240 has been obtained for a 3-layers MoS₂ ribbon, exceeding the values of other 2D based strain sensors.

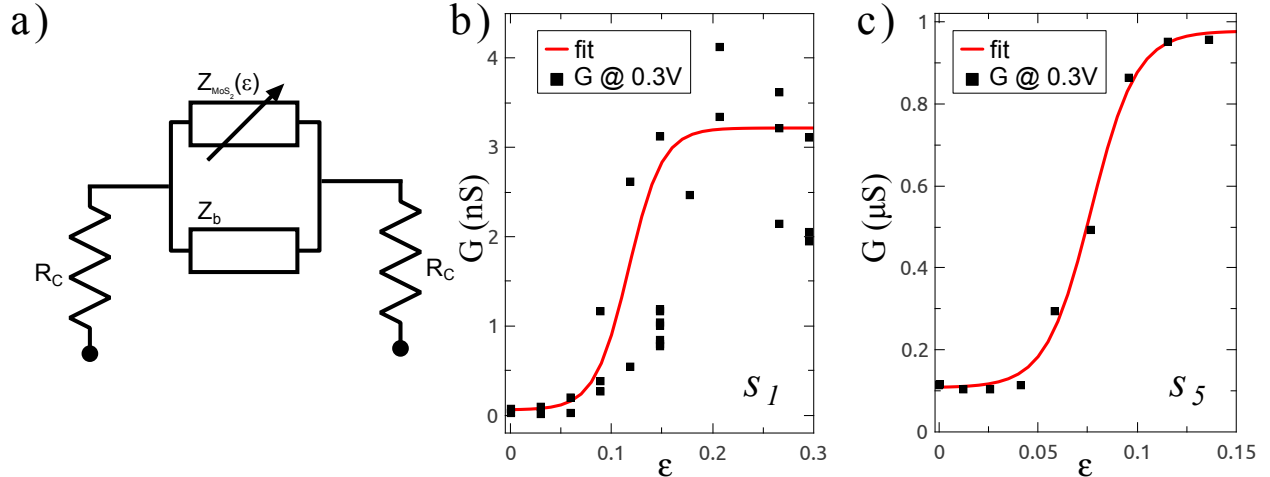


FIG. 5. Conductance of the device. a) Equivalent circuit of the device formed by two ohmic contacts in series with the strain dependent impedance of the MoS₂ flake and a background impedance. b) Measured (black squares) and modeled (solid red line) conductance of the device at $V_p=300$ mV.

The observed increase in electronic transport is compatible with band-gap closure induced by strain, as suggested by previous *ab initio* studies. The rate at which the band-gap is reduced, is estimated with a sound model of the conductance as function of the applied strain, obtaining data between -31 and -45 meV/%strain, close to the theoretical prediction. The results and the methodology shown in this work pave the way for the development of new devices at micro and nano-scale which exploit electro-mechanical coupling of MoS₂.

AUTHOR CONTRIBUTIONS

I.N. and M.L.S. contributed equally to this work.

ACKNOWLEDGMENTS

The authors gratefully acknowledge W. Venstra for useful discussion, S. Tacchi for AFM measurements. The authors acknowledge financial support from the European Commission (FPVII, Grant agreement no: 318287, LANDAUER).

REFERENCES

- [1] M. Hempel, D. Nezich, J. Kong, and M. Hofmann, *Nano letters* **12**, 5714 (2012).
- [2] Z. A. Boeva and T. Lindfors, *Sensors and Actuators B: Chemical* **224**, 624 (2016).
- [3] F. R. Fan, W. Tang, and Z. L. Wang, *Advanced Materials* **28**, 4283 (2016).
- [4] L. Shen, Q. Che, H. Li, and X. Zhang, *Advanced Functional Materials* **24**, 2630 (2014).
- [5] S. Bertolazzi, J. Brivio, and A. Kis, *ACS nano* **5**, 9703 (2011).
- [6] Q. H. Wang, K. Kalantar-Zadeh, A. Kis, J. N. Coleman, and M. S. Strano, *Nature nanotechnology* **7**, 699 (2012).
- [7] W. Wu, L. Wang, Y. Li, F. Zhang, L. Lin, S. Niu, D. Chenet, X. Zhang, Y. Hao, T. F. Heinz, J. Hone, and W. Zhong Lin, *Nature* **514**, 470 (2014).
- [8] K.-A. N. Duerloo, M. T. Ong, and E. J. Reed, *The Journal of Physical Chemistry Letters* **3**, 2871 (2012).
- [9] H. Zhu, Y. Wang, J. Xiao, M. Liu, S. Xiong, Z. J. Wong, Z. Ye, Y. Ye, X. Yin, and X. Zhang, *Nature nanotechnology* **10**, 151 (2015).
- [10] E. Scalise, M. Houssa, G. Pourtois, V. Afanasev, and A. Stesmans, *Nano Research* **5**, 43 (2012).
- [11] P. Johari and V. B. Shenoy, *ACS nano* **6**, 5449 (2012).
- [12] M. Ghorbani-Asl, S. Borini, A. Kuc, and T. Heine, *Physical Review B* **87**, 235434 (2013).
- [13] H. J. Conley, B. Wang, J. I. Ziegler, R. F. Haglund Jr, S. T. Pantelides, and K. I. Bolotin, *Nano letters* **13**, 3626 (2013).
- [14] W. S. Yun, S. Han, S. C. Hong, I. G. Kim, and J. Lee, *Physical Review B* **85**, 033305 (2012).
- [15] M. López-Suárez, I. Neri, and R. Rurali, *Journal of Applied Physics* **119**, 165105 (2016).
- [16] N. Kaushik, A. Nipane, F. Basheer, S. Dubey, S. Grover, M. M. Deshmukh, and S. Lodha, *Applied Physics Letters* **105**, 113505 (2014).
- [17] H. Li, J. Wu, Z. Yin, and H. Zhang, *Accounts of chemical research* **47**, 1067 (2014).
- [18] H. Li, Z. Yin, Q. He, H. Li, X. Huang, G. Lu, D. W. H. Fam, A. I. Y. Tok, Q. Zhang, and H. Zhang, *small* **8**, 63 (2012).

- [19] A. Castellanos-Gomez, M. Buscema, R. Molenaar, V. Singh, L. Janssen, H. S. van der Zant, and G. A. Steele, *2D Materials* **1**, 011002 (2014).
- [20] A. Castellanos-Gomez, R. Roldán, E. Cappelluti, M. Buscema, F. Guinea, H. S. J. van der Zant, and G. A. Steele, *Nano Letters* **13**, 5361 (2013).
- [21] J. Quereda, J. J. Palacios, N. Agrait, A. Castellanos-Gomez, and G. Rubio-Bollinger, *2D Materials* **4**, 021006 (2017).
- [22] K. He, C. Poole, K. F. Mak, and J. Shan, *Nano letters* **13**, 2931 (2013).
- [23] S. Manzeli, A. Allain, A. Ghadimi, and A. Kis, *Nano letters* **15**, 5330 (2015).
- [24] M. Huang, T. A. Pascal, H. Kim, W. A. Goddard III, and J. R. Greer, *Nano letters* **11**, 1241 (2011).